Complexity Project: The Oslo Model

CID: 01807529

17th February, 2020

Abstract: The aim of this project is to study self-organized criticality and finite-size scaling in the Oslo model: a boundary-driven one-dimensional BTW model in which the threshold slope z_i^{TH} is chosen randomly between 1 and 2 after the relaxation of the site i. The remarkable feature of this model is that it self-organizes into a steady state displaying scale-free behavior in the response of the system to small perturbations. The complexity exhibited by the system is not contained in the algorithm used to define it, but rather, it is the result of the few simple interaction rules defined in the algorithm for local dynamical variables.

Word count: 2700 words.

Contents

1 Introduction

This project is divided into four main sections: in section 3, the computer program that implements the Oslo model is tested, and the relevant results are reported. Once verified the correct functioning of the program, the behavior of $h(t; L)$, namely the height of the pile at site $i = 1$, and the scaling of the cross-over time, namely the time at which the first grain leaves the system, have been investigated. In particular, the expected behavior is compared with the one obtained numerically by means of polynomial regressions and by performing a data collapse. In section 4, the numerical data for $\langle h(t; L)\rangle_t$ have been used to reveal corrections to scaling introduced by the finite size of the systems considered. After that, we focus on the probability distribution and the standard deviation of $h(t; L)$ of systems in their steady state, namely when the average influx of grains equals the average outflux. A data collapse for the probability densities has been performed. The last section investigates the avalanche-size probability density $P(s; L)$ of systems of different sizes once they have self-organized themselves into a critical state. The aim is to check whether $P(s; L)$ are consistent with a finite-size scaling ansatz. In order to do so, the critical exponents that appear in the ansatz have been evaluated by means of a qualitative analysis of the data collapse and by a quantitative analysis of the statistical momenta.

2 Implementation of the Oslo model: testing the program

In order to test whether the implementation of the model works correctly, four tests have been performed. As suggested in the notes, the average height of the pile at site $i = 1$ for system sizes 16 and 32, once they have reached the steady state should be about 26.5 and 53.9. The test is performed by adding 50000 grains to the system in the steady state. The results are summarized in table 1.

L	Grains added	$\langle h(t; L)\rangle_t$
16	50000	26.54
32	50000	53.91

Table 1: Test: average height for $L = 16, 32$. The expected values are 26.5 and 53.9

The second test is qualitative: by using different probabilities, the height of the pile for a system of size $L = 64$ has been plotted. We expect to see no changes in the height of the pile for $p = 0$ and $p = 1$ (where $P(z^{TH} = 1) = p$ and $P(z^{TH} = 2) = 1 - p$) once the system has reached the steady configuration. In particular, the height of the pile for $p = 0$ and $p = 1$ must be L and $2L$, respectively. We expect to see the average height growing as p goes from 1 to 0 (figure 1).

The third test concerns the average avalanche size: once reached the attractor of the dynamics the average number of grains added must be equal to the average number of

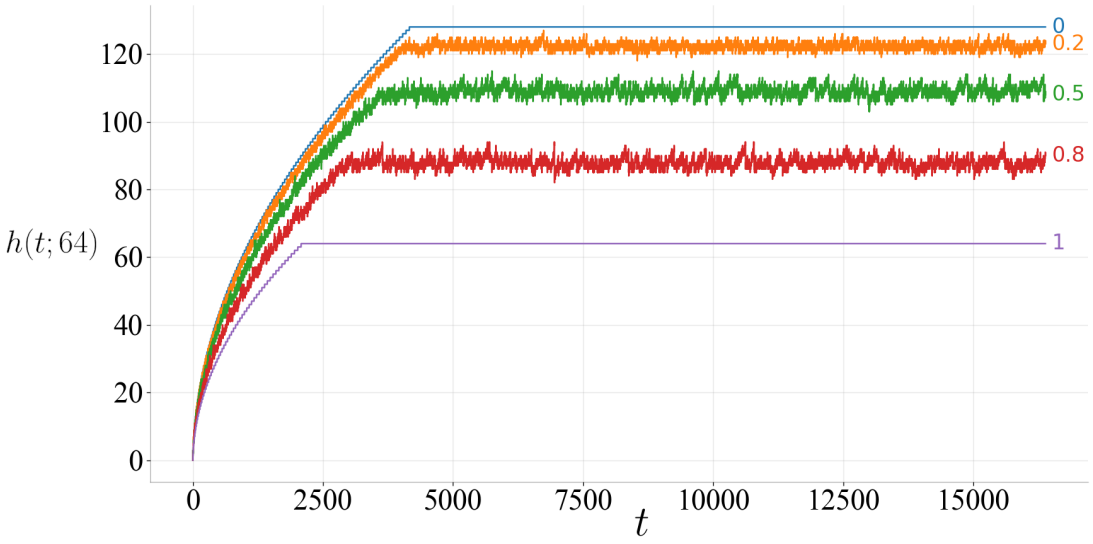

Figure 1: $h(t;L)$ vs. t for $L = 64$, for $p = 0, 0.2, 0.5, 0.8, 1$ where $P(z^{TH} = 1) = p$ and $P(z^{TH} = 2) = 1 - p$.

grains that leave the system; since grains are added to the site $i = 1$, the average avalanche size in a system of size L in the steady state must be L. The results are listed in table 2.

L	Number of avalanches observed	$\langle s \rangle$
8	50000	8.000
16	50000	15.997
32	50000	32.020
64	50000	64.062
128	50000	127.967

Table 2: Test: avarage avalanche sizes

The last test is based on the fact that the number of recurrent configurations in a system of size L is

$$N_R = \frac{1}{\sqrt{5}}\left(\phi(1+\phi)^L + \frac{1}{\phi(1+\phi)^L}\right). \tag{1}$$

In particular, for $L = 1, 2, 3, 4$ there are 2, 5, 13, 34 recurrent configurations respectively. Once reached the steady state, the number of different configurations visited by the system has been counted. Table 3 summarizes the parameters used and the results obtained.

L	Expected N_R	$N_R(200)$	$N_R(10k)$	$N_R(50k)$	$N_R(100k)$	$N_R(200k)$
1	2	2	2	2	2	2
2	5	5	5	5	5	5
3	13	11	13	13	13	13
4	34	20	32	34	34	34

Table 3: Test: number of recurrent configurations for a system of size L in the steady state. N_R is the number of recurrent configurations; $N_R(n)$ is the number of different observed configurations in a set of n configurations observed.

3 Height of the pile and cross-over time

This part of the project investigates the behavior of the height of the pile and the cross-over time: consider a system of size L, the height of the pile, that is the number of grains in the first site, is

$$h(t;L) = \sum_{i=1}^{L} z_i(t) = (h_1(t) - h_2(t)) + (h_2(t) - h_1(t)) + \cdots + (h_L(t) - h_{L+1}(t)) = h_1(t), \quad (2)$$

where t is the discrete time measured in units of grains added. The cross-over time $t_c(L)$ is defined as the number of grains in the system (of size L), before an added grain induces, for the first time, a relaxation at site $i = L$.

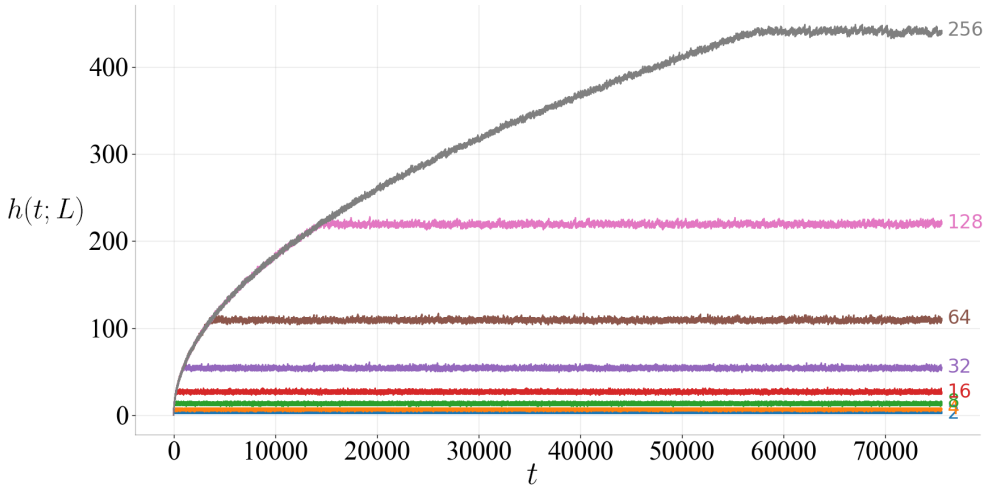

Figure 2: $h(t;L)$ vs. t for $L = 2, 4, \ldots, 64$ starting from the empty configuration ($z_i = 0\ \forall i$).

To make the program more efficient, however, $h(t;L)$ is not measured using equation 2: the height at site $i = 1$ only changes when a grain is added and when the site topples,

therefore, by keeping track of these changes, the computationally expensive equation 2 can be avoided.

Figure 2 shows the $h(t;L)$, starting from an empty system (t=0), for $L = 2$, 4, 8, 16, 32, 64, 128, 256.

A configuration $S_j = \{z_1, z_2, \ldots, z_{L-1}, z_L\}$ for a system of size L is stable if all the local slopes do not exceed the local threshold slope, i.e. if $z_i < z_i^{TH}\ \forall i = 1, \ldots, L$. The set of all the stable configurations $S = \{S_j\}$ can be divided into two sets: T and R, such as $S = T \cup R$ and $T \cap R = \emptyset$. T is the set of transient configurations, while R is the set of recurrent configurations. T is defined as the set of all the configurations that are encountered at most once during the evoloution of the system, whereas R is the set of all the configurations that can be encountered an indefinite number of times. Symbolically the evolution of the system from one stable configuration to another can be written as $S_j \to S_{j+1}$, and the evolution of a system, starting from a transient configuration, is $T_0 \to T_1 \to \cdots \to T_{n-1} \to R_n \to R_{n+1} \to \ldots$. In this sense, the set of recurrent configurations is said to be the attractor of the dynamic in the space of all the configurations. For any stable configuration $L+1-i \leq h_i \leq 2(L+1-i)\ \forall i$, these two limit shapes are the staircase configurations with $z_i = 1\ \forall i$ and $z_i = 2\ \forall i$ respectively. In figure 2, while the system is in T, the height of the piles rises. After that, the system enters the set R of recurrent configurations and eventually, it reaches a steady state for which the number of grains added equals, on average, the number of grains that topple out of the system. The height of the pile continues to rise for a certain amount of time after the system has entered the set of stable configurations. This is due to the fact that although the threshold slopes are chosen randomly after every relaxation, they do not appear with equal probability in stable configurations. Even though in principle, the system could visit all the recurrent configurations, the probability for some of them to be visited is low. The cross-over time and the time at which the system enters the set of recurrent configurations can be distinct.

3.1 Theoretically

Let $h(t;L)$ be the height of the pile of a system of size L once it has reached the steady state and let $t_c(L)$ be the cross-over time. Given a configuration $S = \{z_i\}$, the height of the pile can be written as:

$$\langle h(t;L)\rangle_t = \frac{1}{T}\sum_{t=t_0+1}^{T}\sum_{i=1}^{L} z_i(t) = \sum_{i=1}^{L}\langle z\rangle_t = \langle z\rangle_t L, \tag{3}$$

Where we assumed $\langle z_i\rangle = \langle z\rangle$. The cross-over time can be written as:

$$t_c^j(L) = \sum_{i=0}^{L} z_i^j i, \tag{4}$$

with $S^j = \{z_i^j\}$ the configuration of the j^{th} realization of the system one unit of time before an added grain induces for the first time the relaxation of the site $i = L$. The average cross-over time $\langle t_c(L)\rangle$ is:

$$\langle t_c(L)\rangle = \frac{1}{M}\sum_{j=1}^{M}\sum_{i=0}^{L} z_i^j i = \langle z\rangle \sum_{i=0}^{L} i = \langle z\rangle \frac{L(L+1)}{2} = \frac{\langle z\rangle}{2} L^2\left(1+\frac{1}{L}\right), \tag{5}$$

where we suppose that the average height of the pile in the steady state is equal to the height of the pile at the cross-time, so that for equations 3 and 5, $\langle z\rangle_t = \langle z\rangle$. The expected behavior of the cross-over time and the average height of the system in the steady state is:

$$\begin{aligned} \langle h(t;L)\rangle_t &= \sum_{t=t_0+1}^{t_0+T} h(t;L) \propto L \\ \langle t_c(L)\rangle &= \sum_{j=1}^{M} t_c^j(L) \propto L^2 \end{aligned} \tag{6}$$

Even though $1 \leq \langle z\rangle \leq 2$, this value depends on L for small values of L so that the behavior of $\langle h(t;L)\rangle_t$ and $\langle t_c(L)\rangle$ is not perfectly linear, as investigated in the next sections.

3.2 Numerically

Figure 3 shows the scatter plot of cross-over times $\langle t_c(L)\rangle$, obtained numerically by averaging over $M = 10$ different realizations of systems of sizes $L = 2, 4, \ldots, 256, 512$, together with the polynomial fit. The cross-over time is expected to scale as $\langle t_c(L)\rangle \propto L^2$ for $L \gg 1$, therefore, a fit for the set of points $\{(L, \langle t_c(L)\rangle),\ L \geq 16\}$, with the function $c_0 + c_1 L + c_2 L^2$ has been performed. Figure 4 shows the average heights of the pile $\langle h(t;L)\rangle_t$ vs. L for $L = 2, 4, \ldots, 256, 512$, together with the linear regression line for the set of points $\{(L, \langle h(t;L)\rangle_t),\ L \geq 16\}$. $\langle h(t;L)\rangle_t$ is evaluated using equation 3 with $t_0 = L^2$.

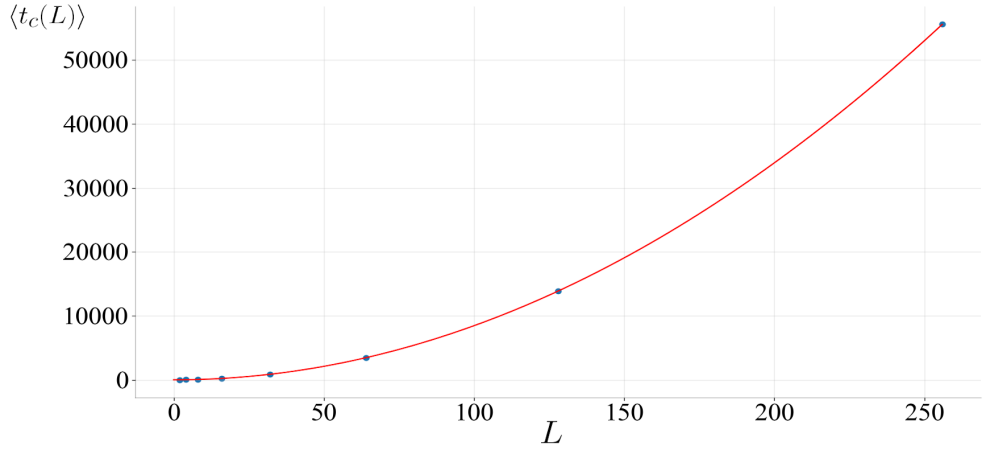

Figure 3: Scatter plot of $\langle t_c(L)\rangle$ vs. L for $L = 2, 4, 8, 16, 32, 64, 128, 256$ averaged over $M = 10$ realizations, together with the second-degree polynomial fit. The best-fitting line is: $3.77 - 0.48x + \mathbf{0.85}x^2$

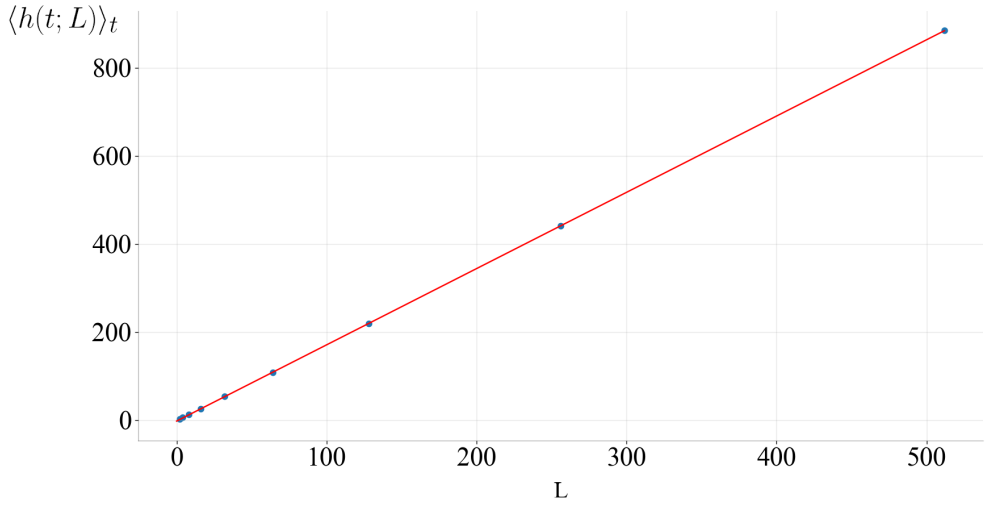

Figure 4: Scatter plot of $\langle h(t;L)\rangle_t$ (for T=20000) vs. L for $L = 2, 4, 8, 16, 32, 64, 128, 256$, together with the regression line obtained for points with $L \geq 16$. The slope of the regression line is **1.73**.

The parameters $\frac{\langle z\rangle}{2} = 0.85$ and $\langle z\rangle = 1.73$ are compatible with each other.

3.3 Data collapse

The data collapse is performed by introducing the scaling function $\mathcal{F}$:

$$h(t;L) = \langle z\rangle L \mathcal{F}\left(\frac{t}{t_c(L)}\right), \tag{7}$$

so that by plotting $h(t;L)$ vs. the rescaled time $\frac{t}{t_c(L)}$, the corss-over times are horizontally aligned as shown in figure 5 (a). The data collapse is obtained by plotting $\frac{h(t;L)}{L}$ vs. the rescaled time $\frac{t}{t_c(L)}$. The function $\mathcal{F}$ depends on the rescaled variable $x = \frac{t}{t_c(L)}$ and its behavior is:

$$\mathcal{F}(x) = \begin{cases} \sqrt{x} & , x \leq 1 \\ 1 & , x > 1 \end{cases}$$

Figure 5 shows the data collapse for the smoothed heights

$$\tilde{h}(t;L) = \frac{1}{M}\sum_{j=1}^{M} h^j(t;L), \tag{8}$$

where $h^j(t,L)$ is the j^{th} realization of the system (starting from the empty configuration at t=0).

The fact that $\langle t_c(L)\rangle \propto L^2$ for $L \gg 1$ implies that the height of the pile (for which $\langle h(t;L)\rangle \propto L$) during the transient grows as $\tilde{h}(t;L) \propto \sqrt{t}$. This growth, for $t < t_c(L)$ must be independent of L: as long as the site $i = L$ remains empty, the finite size of the

system does not affect its evolution in any way. For $t < t_c(L)$ the L that multiplies the scaling function cancels out with the L^2 in the denominator of the rescaled time. For $t > t_c$, $\langle h(t;L)\rangle_t$ is a constant proportional to L.

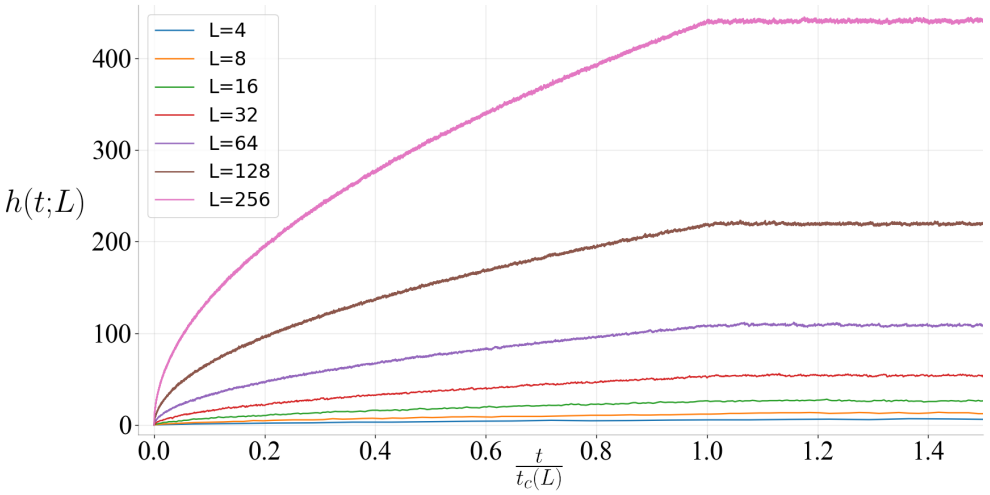

(a)

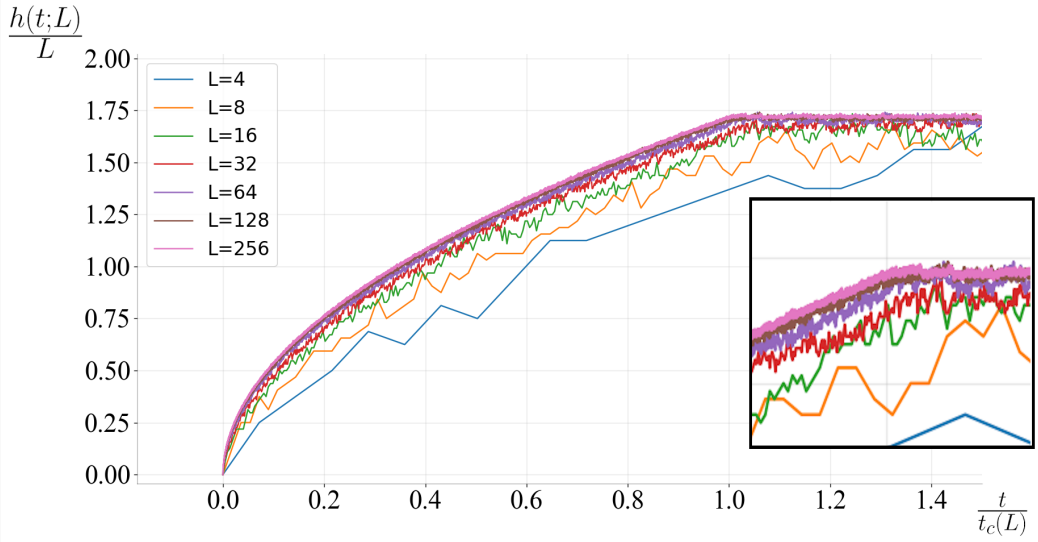

(b)

Figure 5: (a) horizontally aligned cross-over times: $\tilde{h}(t;L)$ $(M = 5)$ vs. the rescaled time $\frac{t}{t_c(L)}$ (b) data collapse: $\frac{\tilde{h}(t;L)}{L}$ $(M = 5)$ vs. the rescaled time $\frac{t}{t_c(L)} = \frac{t}{\frac{\langle z\rangle}{2}L^2} = \frac{t}{0.85L^2}$.

4 Scaling of the average height, and probability distribution

Let $\langle h(t;L)\rangle_t$ be the average height of the pile for times $t > t_0$ (equation 3), that is, the system has reached the steady state. We will consider the standard deviation

$$\sigma_h(L) = \sqrt{\langle h^2(t;L)\rangle_t - \langle h(t;L)\rangle_t^2}, \tag{9}$$

and the normalized height probability

$$\begin{aligned} P(h;L) &= \frac{\text{Number of observed configurations with height h in system of size L}}{T_h\text{=Total number of observed configurations}}, \\ \sum_{h=0}^{\infty} P(h;L) &= 1 \end{aligned} \tag{10}$$

4.1 Corrections to scaling

We assume the form

$$\langle h(t;L)\rangle_t = a_0 L(1 - a_1 L^{-\omega_1} + a_2 L^{-\omega_2} + \dots), \tag{11}$$

with $\omega_i > 0$ and a_i constants. An estimate for a_0 is given by the linear fit for the points $(L, \langle h(t;L)\rangle_t)$ with L sufficiently large so that the non-linear terms become negligible, as done in section 3.2 (figure 4).
To estimate ω_1 we consider the points $(\log L, \log \frac{-\langle h(t;L)\rangle_t)+1}{a_0 L})$ and we perform a linear fit for them. The slope of the regression line is an estimate for $-\omega_1$. Figure 6 shows the scatter plot for $L = 2, 4, 8, 16, 32, 64, 128, 256$ together with the regression line.

The exponent of the first correction term is then $\omega_1 = 0.69$.
Another way to estimate a_0 is by directly fitting $\frac{\langle h(t;L)\rangle_t}{L}$ with the function $a_0(1 - a_1 L^{-\omega_1})$ as shown in figure 7.

The parameters evaluated with this latter method are consistent with the ones of the regression lines:

Parameters	Linear fit	Nonlinear fit
a_0	1.73	1.73
ω_1	0.69	0.64

Table 4: Corrections to scaling: parameters evaluated using the two different methods

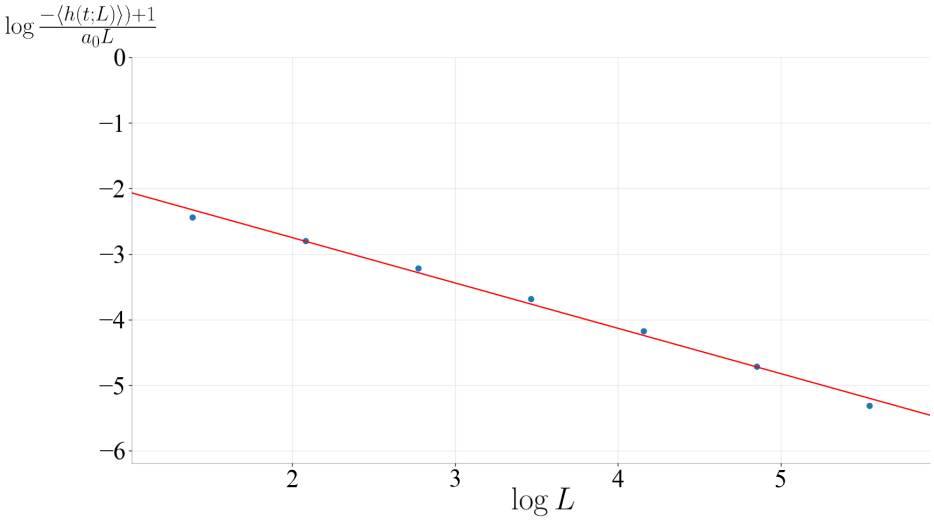

Figure 6: scatter plot for the points $(\log L, \log \frac{-\langle h(t;L)\rangle)+1}{a_0 L})$ for $L = 2, 4, 6, 16, 32, 64, 128, 256$ together with the regression line. The slope of the regression line is **-0.69**. log in the naturam logarithm

4.2 Standard deviation

Figure 8 shows the values of the standard deviation $\sigma_h(L)$ for system sizes $L = 2, 4, \ldots, 128, 256$.

4.3 Probability distribution

Consider $h = \sum_{i=1}^{L} z_i$. Let's assume that z_i are independent, identically distributed random variables with finite variance. The central limit theorem establishes that the (normalized) distribution of the sum tends toward a normal distribution as L grows, regardless of the distribution of the individual z_i. In particular, if the expected value of z_i is $E[z_i] = \mu$ and the variance is $Var[z_i] = \sigma^2 < \infty$ then the expected value of h, $E[h]$ and the variance $Var[h]$ are

$$\begin{aligned} E\left[\sum_{i=1}^{L} z_i\right] &= \sum_{i=1}^{L} E[z_i] = L\mu \\ Var\left[\sum_{i=1}^{L} z_i\right] &= \sum_{i=1}^{L} Var[z_i] = L\sigma^2. \end{aligned} \tag{12}$$

Equation 12 holds true only if $Cov[z_i, z_j] = 0 \ \forall i, j = 1, \ldots L$, namely if the variables are independent. Figure 9 shows $\log \sigma_h(L)$ vs. $\log L$, together with the regression line. For independent, identically distributed random variables we expect

$$\log \sigma_h(L) = \log L^{\frac{1}{2}} \sigma = \frac{1}{2} \log L + const \tag{13}$$

Since the slope of the regression line is $0.24 \neq 0.5$, the hypothesis of independent variables is not satisfied by the numerical results.

In the limit $L \to \infty$ the average slope $\sum_{i=1}^{L} z_i \to \frac{\langle h(t;L)\rangle_t}{L} \to a_0$.

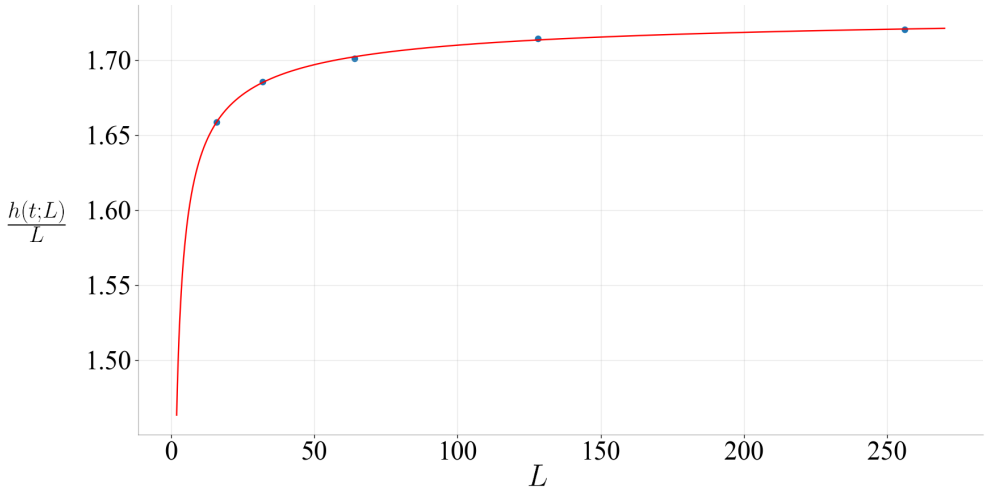

Figure 7: scatter plot for the foints $(L, \frac{\langle h(t;L)\rangle}{L})$ for $L = 16, 32, 64, 128, 256$ together with the best-fitting function of the form $a_0(1 - a_1 L^{-\omega_1})$. The parameters are $a_0 = \mathbf{1.73}$, $a_1 = 0.25$, $\omega_1 = \mathbf{0.64}$.

4.4 Data collapse for $P(h; L)$

If we suppose that z_i are independent, identically distributed random variables then $h = \sum_{i=1}^{L} z_i$, for large L, is normally distributed. Figure 10 shows $P(h; L)$ (equation 10) for $L = 8, 16, 32, 64, 128, 256$ with $T_h = 50000$.

To perform a data collapse, we plot $\sigma_h(L)P(h; L)$ vs. the exponent $\frac{h-\mu}{\sigma}$ to cancel out the standard deviation that appears in the coefficient of the normal distribution, and to align the distributions horizontally:

$$N(h, \mu, \sigma) \propto \frac{1}{\sigma} e^{\left(\frac{h-\mu}{\sigma}\right)^2} \tag{14}$$

Figure 11 shows the data collapse for $L = 2, 4, \ldots, 256$ with $T_h = 50000$.

5 The avalanche-size probability

This section investigates the avalanche size probability for systems of different sizes L once they have reached the steady configuration: from a sample of N avalanches $s_1, s_1, s_1, \ldots$ we define

$$\begin{aligned} P_N(s; L) &= \frac{\text{Number of avalances of size } s_i = s}{N}, \\ \sum_{h=0}^{\infty} P(s; L) &= 1. \end{aligned} \tag{15}$$

The size of an avalanche is the number of relaxation induced by the addition of one grain at the site $i = 1$, including the avalanches of size $s = 0$ when no relaxation is

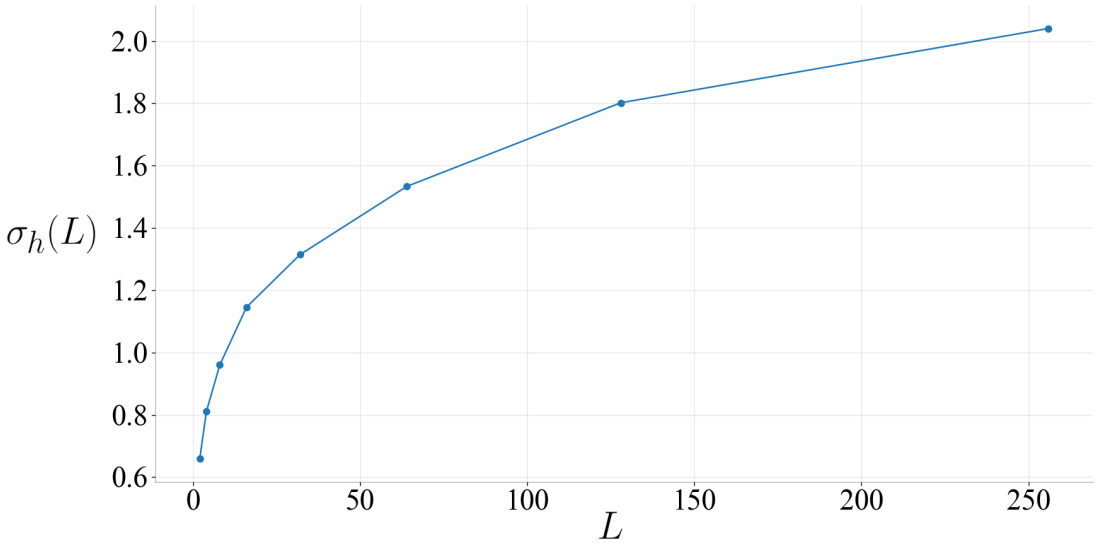

Figure 8: Standard deviation $\sigma_h(L)$ for system sizes $L = 2, 4, \ldots, 128, 256$

induced.

5.1 Log-binnined data

For a critical system, roughly speaking, the majority of the events are small events, and large events are very rare. For this reason, the tail of the distribution appears to be noisy. We can extract information from the tail of the observed distribution by binning the data. We can divide the s-axis into bins of exponentially increasing length: the j^{th} bin will cover the interval $[a^j, a^{j+1}[$, with $a > 1$. The avalanche size probability for binned data is defined as

$$\tilde{P}_N(s^j; L) = \frac{\text{Number of avalances of size } s \in [s^j_{min}, s^j_{max}]}{N\Delta s^j}, \tag{16}$$

where s^j_{min}, s^j_{max} are the mininimum and maximum integers in bin j and

$$\begin{aligned} \Delta s^j &= (s^j_{max} - s^j_{min} + 1) \text{ is the number of integers in the interval,} \\ s^j &= \sqrt{s^j_{max} s^j_{min}}. \end{aligned} \tag{17}$$

Figure 12 shows the avalanche-size probability for $L = 30$, $N = 5000, 50000$ together with the same probability obtained from log-binned data choosing $a = 1.2$. For the two different N the statistics is not enough to explore the probability of events that are less than $\sim 1/N$ likely to happen.

Samples of $N = 100000$ avalanches has been taken for system sizes $L = 4, 8, 16, 32, 64, 128, 256, 512$ in their steady states. The relative log-binned ($a = 1.2$) avalanche-size probabilities are plotted in figure 13. The avalanche-size probability follows a power-law decay; thus, a log-log plot is the most suitable to appreciate this behavior.

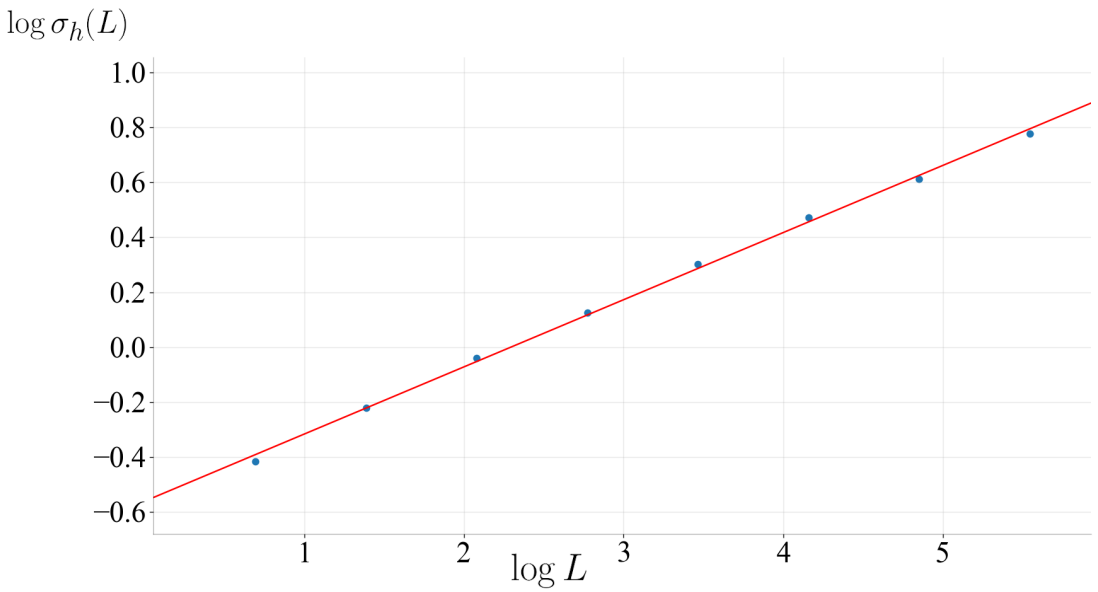

Figure 9: $\log \sigma_h(L)$ vs. $\log L$ for system sizes $L = 2, 4, \ldots, 128, 256$. The slope of the regression line is **0.24**. log in the naturam logarithm

5.2 Data collapse

To test if $\tilde{P}_N(s; L)$ is consistent with the scaling ansatz

$$\tilde{P}_N(s; L) \propto s^{-\tau_s} \mathcal{G}\left(\frac{s}{s_c(L)}\right) \qquad (18)$$
$$s_c(L) \propto L^D$$

for $L \gg 1$, $s \gg 1$, and estimate the values of the avalanche dimension D and the avalanche-size exponent τ_s a data collapse has been performed. Plotting (in a log-log plot) the transformed avalanche-size probabilities $s^{\tau_s}\tilde{P}_N(s; L)$ vs. s, the rapid decay of each graph is vertically aligned. To align the decays of the graphs horizontally, we plot the transformed avalanche-size probability vs. the rescaled avalanche size. In the next section, the values of these two parameters will be numerically estimated with the moment analysis method; now, their value is inferred from a qualitative analysis of the goodness of the data collapse. Figure 14 and 18 (last page) report three attempts to the data collapse togheter with the values of the parameters used. The critical exponents have been varied about $\tau_s = 1.55...$ and $D = 9/4 = 2.25$ that are the conjectured critical exponents for the Oslo model.

The quality of the data collapse indicates that the avalanche-size probability satisfies the scaling ansatz 18 for large system sizes and large avalanche sizes.

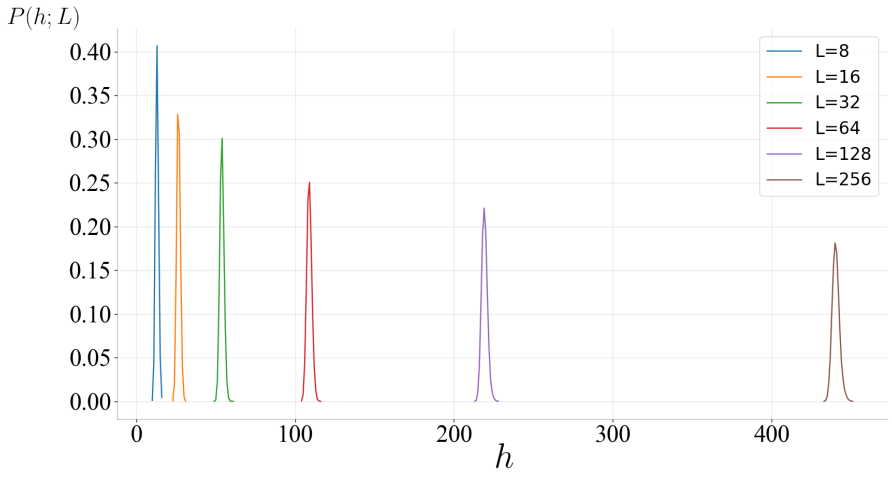

Figure 10: $P(h;L)$ vs. h for $L = 8, 16, 32, 64, 128, 256$ with $T_h = 50000$ (equation 10).

5.3 Moment scaling analysis

The k^{th} moment of the avalanche-size probability is defined as

$$\langle s^k \rangle = \sum_{s=1}^{\infty} s^k P(s;L). \tag{19}$$

The k^{th} moment can be estimated from a sufficiently large sample of avalanche sizes as

$$\langle s^k \rangle = \frac{1}{T} \sum_{t=t_0}^{T} s_t^k \tag{20}$$

where s_t is the avalanche size measured at time t for $t > t_c$. Assuming that the finite-size scaling ansatz of equation 18 is valid for all avalanche sizes we find

$$\begin{aligned}
\langle s^k \rangle =& \sum_{s=1}^{\infty} s^k P(s;L). \\
=& \sum_{s=1}^{\infty} s^k s^{-\tau_s} \mathcal{G}\left(s/L^D\right) \\
\propto& \int_1^{\infty} s^{k-\tau_s} \mathcal{G}\left(s/L^D\right) ds \\
=& \int_{1/L^D}^{\infty} (uL^D)^{k-\tau_s} \mathcal{G}(u) L^D du, \; u = s/L^D \\
=& L^{D(1+k-\tau_s)} \int_{1/L^D}^{\infty} u^{k-\tau_s} \mathcal{G}(u) du.
\end{aligned} \tag{21}$$

The integral converges in the lower limit if $\tau_s < 1 + k$. In the scaling ansatz we assume the scaling function $\mathcal{G}(x)$ to be well-behaved for small values of x and to decay rapidly

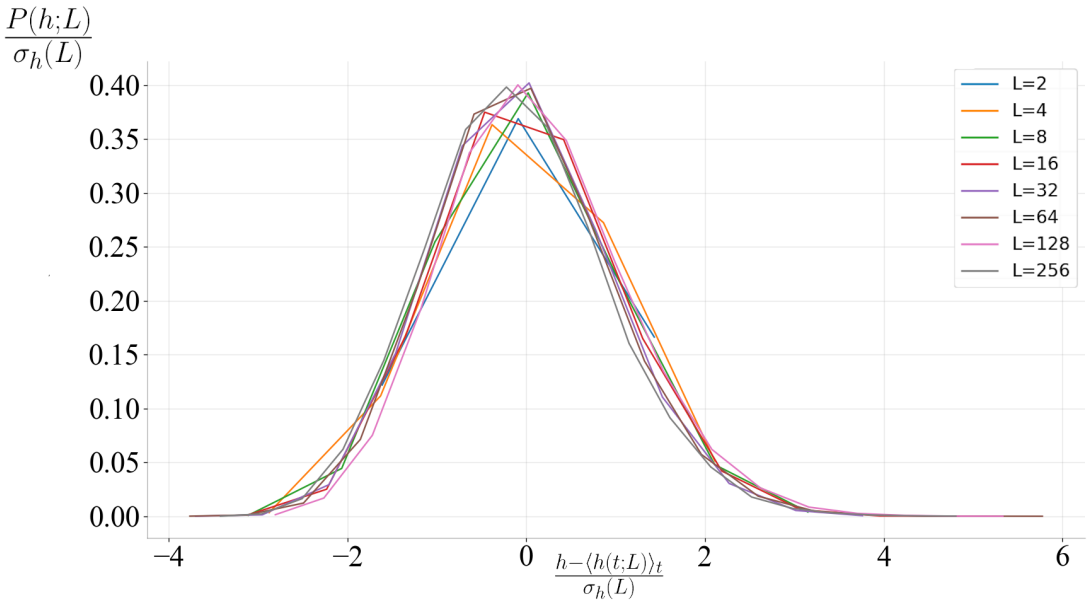

Figure 11: $\sigma_h(L)P(h;L)$ vs. $\frac{h-\langle h(t;L)\rangle_t}{\sigma_h(L)}$ for $T_h = 50000$

for large values of x:

$$\mathcal{G}(x) = \begin{cases} \mathcal{G}(0) + \mathcal{G}'(0)x + \mathcal{G}''(0)x^2 + \dots & \text{for } x \ll 1 \\ \text{decays rapidely} & \text{for } x \gg 1. \end{cases}$$

The rapid decay is indeed assumed in order to have finite moments for finite system sizes, and in particular, the integral in the last expression of equation 21 converges in the upper limit. The integral tends to a constant for $L \to \infty$ and

$$\langle s^k \rangle \propto L^{D(1+k-\tau_s)}. \tag{22}$$

By taking the logarithm of this expression

$$\log \langle s^k \rangle = D(1+k-\tau_s) \log L + \text{constantfor } L \gg 1,\ k \geq 1 \tag{23}$$

An estimate of D and τ_s can be obtained numerically by performing two linear fit: first we plot the logarithm of each k^{th} moment vs. $\log L$ for $k = 1, 2, 3 \dots$. The slope of each graph is an estimate for $D(1 + k - \tau_s)$.Then, by plotting $D(1 + k - \tau_s)$ vs. k we obtain a straight line that intersects the k-axis at the point $\tau_s - 1$ and which slope is an estimate for D. Figure 15 shows the two scatter plot together with the regression lines.

The parameters obtained thorugh this method, $\tau_s = 1.69$ and $D = 2.23$, are consistent with the ones obtained with the data collapse. Again, the good quality of the linear regression indicates that the scaling ansatz for the avalanche-size probability density is satisfied.

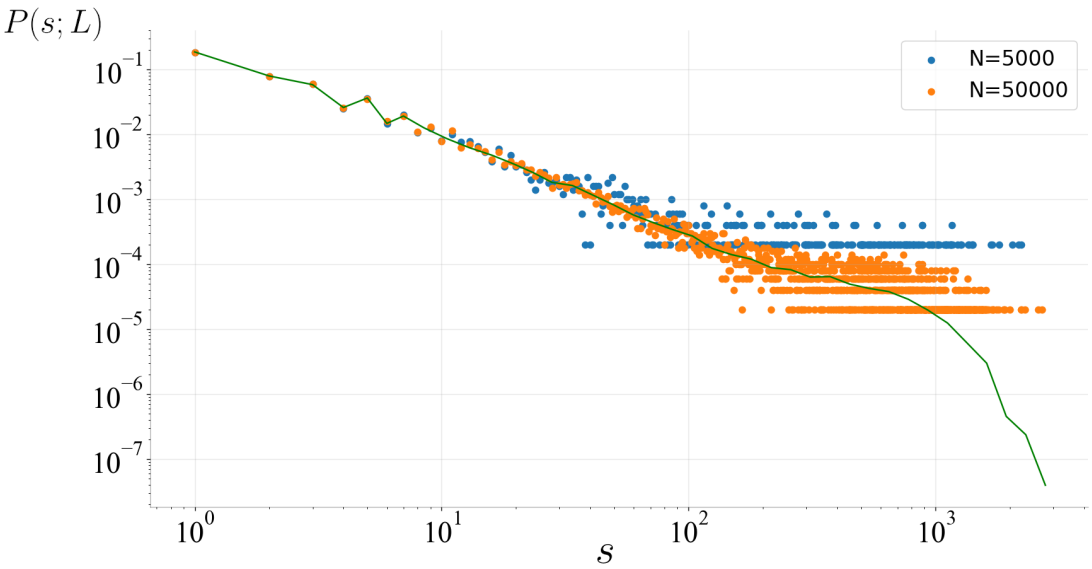

Figure 12: Avalanche-size probability for $L = 30$, $N = 5000, 50000$ together with the same probability obtained from log-binned data choosing $a = 1.2$.

5.4 Corrections to scaling

In the continued equality 21 it turns out that the k^{th} moment is proportional to $L^{D(1+k-\tau_s)}$ for large L. To reveal corrections to scaling, we can look at $\frac{\langle s^k \rangle}{L^{D(1+k-\tau_s)}}$, as done in figure 17. If we assume the scaling ansatz of equation 21 then the plot shows the behavior of the integral $\int_{1/L^D}^{\infty} u^{k-\tau_s}\mathcal{G}(u)du$. As L grows, this term tends to a constant (the constant is smaller as the exponent in the integral grows) as expected. On the other hand, for small values of L it introduces corrections. For this reason, the linear fit has been performed for $L \geq 16$.

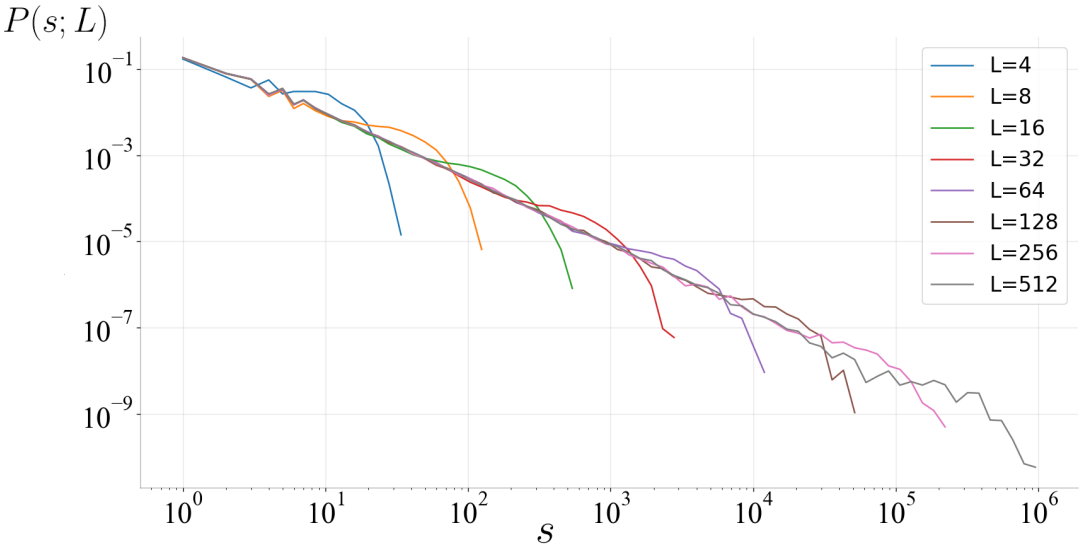

Figure 13: Log-binned avalanche size probabilities from a sample of $N = 100000$ avalanches, for system sizes $L = 4, 8, 16, 32, 64, 128, 256, 512$

Attempts to data collapse

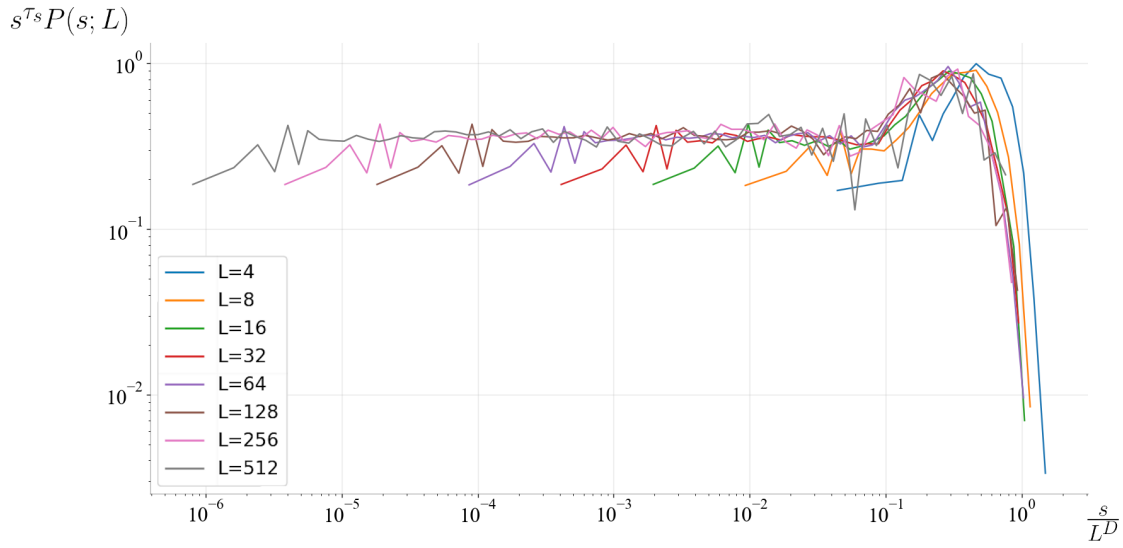

Figure 14: Data collapse of $P(s; L)$ for $L = 4, 8, \ldots, 256, 512$. $\tau_s = 1.55$, $D = 2.25$

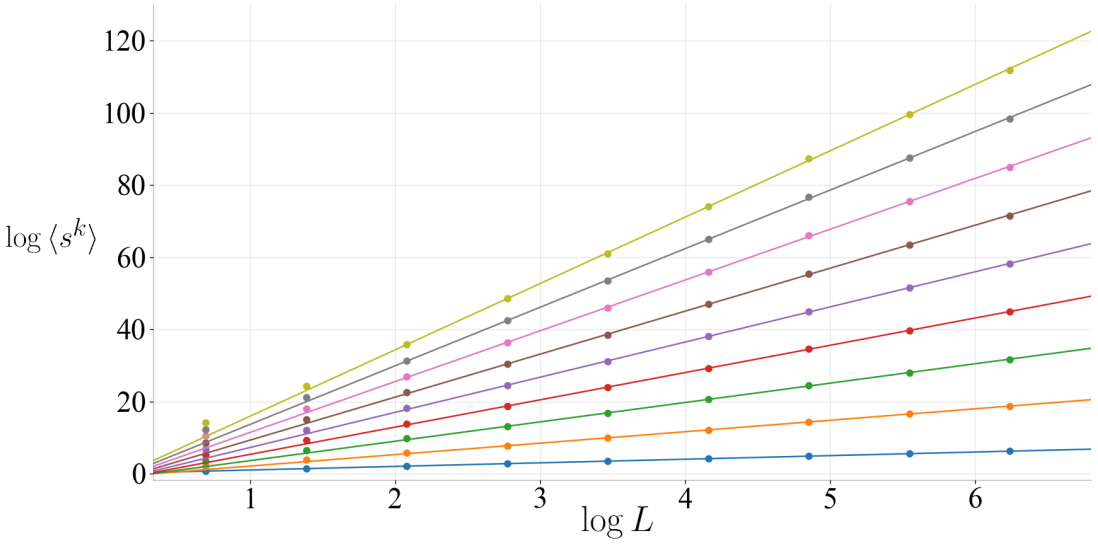

Figure 15: Scatter plot of $\log_e \langle s^k \rangle$ vs. $\log_e L$ together with the regression lines for points with $L \geq 16$. The moments are, starting from below, $k = 1, 2, 3, 4, 5, 6, 7, 8, 9$.

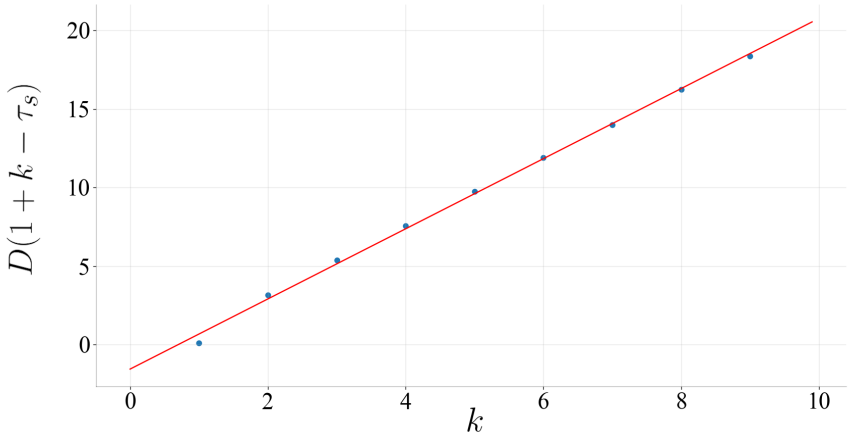

Figure 16: Scatter plot of $D(1+k-\tau_s)$ vs. k, together with the regression line. The slope of the regression line is $D = \mathbf{2.23}$, the intersection with the k-axis is at $k = 0.69$ therefore the avalanche-size exponent is $\tau_s = \mathbf{1.69}$

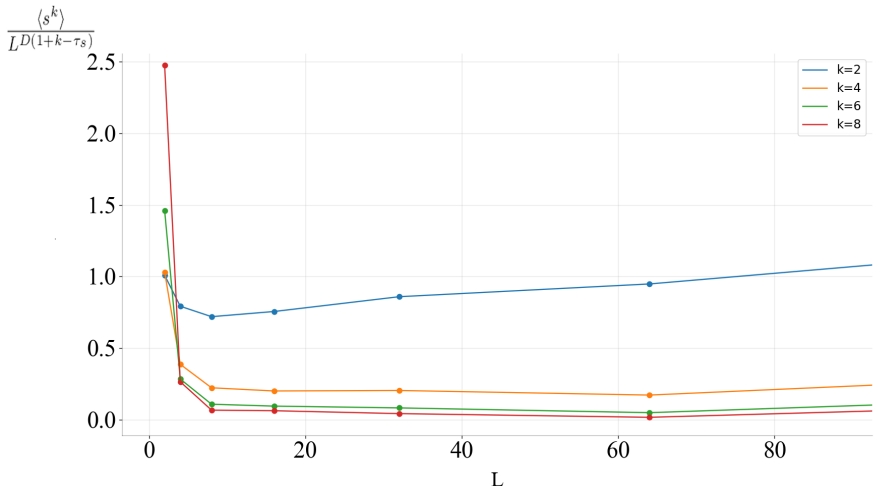

Figure 17: $\frac{\langle s^k \rangle}{L^{D(1+k-\tau_s)}}$ vs. L for $L = 2, 4, 8, 16$. This plot shows the behavior of $\int_{1/L^D}^{\infty} u^{k-\tau_s} \mathcal{G}(u) du$ in order to reveal corrections to scaling for small L. The scaling exponents are the ones found in section 5.3: $D = 2.23$ and $\tau_s = 1.69$.

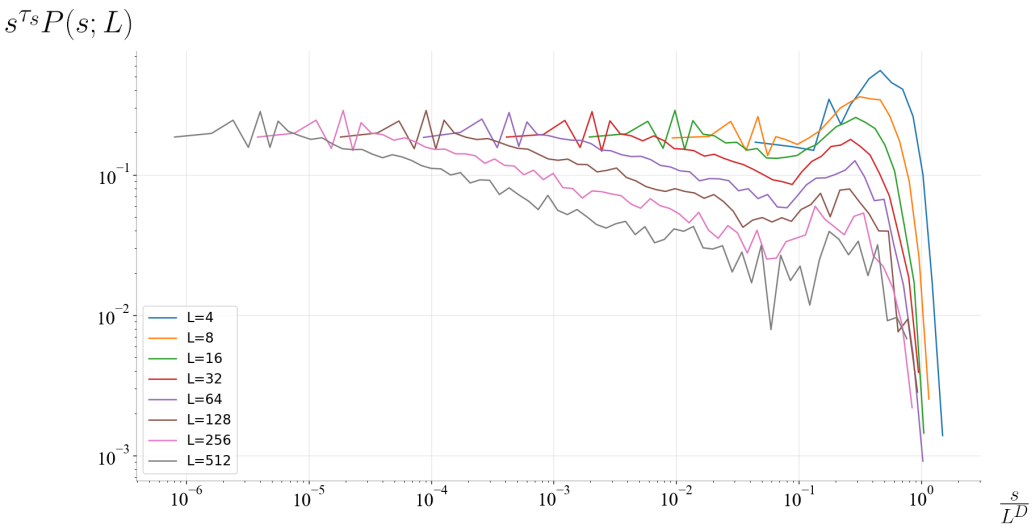

(a)

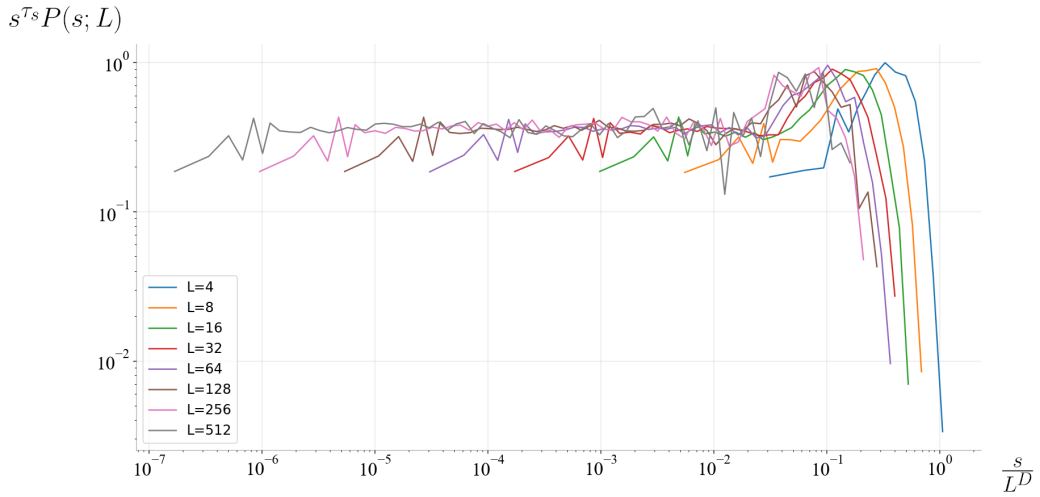

(b)

Figure 18: Data collapse of $P(s;L)$ for $L = 4, 8, \ldots, 256, 512$ with parameters: (a) $\tau_s = 1.3$, $D = 2.25$ (b) $\tau_s = 1.55$, $D = 2.5$